ELSEVIER

Earth and Planetary Science Letters 186 (2001) 231–244

EPSL

www.elsevier.com/locate/epsl

Latest Paleocene–earliest Eocene cyclostratigraphy: using core photographs for reconnaissance geophysical logging

Benjamin S. Cramer *

Rutgers University, Department of Geological Sciences, Piscataway, NJ 08854, USA

Received 27 July 2000; received in revised form 18 January 2001; accepted 18 January 2001

Abstract

I present a new method for reconnaissance cyclostratigraphic study of continuously cored boreholes: the generation of detailed sediment color logs by digitizing Ocean Drilling Program (ODP) core photographs. The reliability of the method is tested by comparison with the spectrophotometer color log for the uppermost Paleocene–lowermost Eocene section (Chron C24r) at ODP Hole 1051A. The color log generated from Hole 1051A core photographs is essentially identical to the spectrophotometer log. The method is applied to the Chron C24r section at Holes 1051A and 690B, producing the first high-resolution geophysical log for the latter section. I calculate astronomically calibrated durations between bio- and chemostratigraphic events within Chron C24r by correlating the cyclostratigraphies for Holes 1051A and 690B. These durations are significantly different from previous estimates, indicating that the chronology of events surrounding the Paleocene/Eocene boundary will have to be revised. This study demonstrates that useful geophysical logs can be generated from digitized ODP and DSDP core photographs. The method is of practical use for sections lacking high-resolution logs, as is the case for most lower Paleogene sections.

Keywords: photographs; color; cycles; cyclostratigraphy; Paleocene; Eocene

1. Introduction

Since the recognition of 'Milankovitch' orbital forcing as the 'pacemaker of the ice ages' [1], cyclostratigraphy has become widely used as a metronome to parse time in the geologic record at a resolution of 10–100 kyr (e.g. [2–4]). Cyclostratigraphy is the only known method useful throughout the geologic record for correlation of the stratigraphic record to a numerical timescale at such a high resolution. Where cyclostratigraphies can be linked to the present, they have superseded radiometric dating as the primary tool for estimating the ages of events in geologic time (e.g. [5,6]).

In marine sections, numerical ages of specific stratigraphic horizons and sedimentation rates between horizons are typically estimated by correlation with the integrated magnetobiochronologic scale of Berggren et al. ([7]; henceforth BKSA95). Essentially, BKSA95 correlates the Cenozoic planktonic foraminiferal and calcareous nannoplankton biozonations via magnetostratig-

* Tel.: +1-732-445-0688; Fax: +1-732-445-3374;
E-mail: bcramer@rci.rutgers.edu

0012-821X/01/$ – see front matter
PII: S0012-821X(01)00249-7

raphy with the geomagnetic polarity timescale of Cande and Kent ([8,9]; henceforth GPTS). The GPTS exploits the seafloor magnetic anomaly pattern and the hypothesis that seafloor spreading rates vary smoothly through time to calibrate the age of magnetic polarity reversals against an interpolated age for the oceanic crust.

The astronomical polarity timescale (APTS) exploits lithologic cycles in sedimentary successions that can be correlated with cycles in the precession, obliquity, and eccentricity of the Earth's orbit around the Sun. The orbital periodicities are physically predictable, and so sedimentary cycles can be correlated with a calculated history of insolation variations [10]. This allows extremely precise dating of magnetic polarity reversals in the sedimentary record, ideally to within a fraction of an average precession cycle ($\sim$21 kyr). Consequently, the APTS was used to constrain the seafloor spreading rate curve from the present to 5.23 Ma in the GPTS.

The Earth's orbit is not fully predictable because of chaotic elements and uncertainties in tidal dissipation [11]. As a result, an APTS constructed by direct correlation with the calculated orbital solution is probably only reliable to $\sim$10 Ma. Alternative methods must be used for older sections. Although more sophisticated methods exist, simple cycle counting using the assumption that cycle durations are similar to the present is a useful first step in evaluating the durations of biochrons estimated in BKSA95 [12]. It must be emphasized that the assumption that cycles reflect orbital forcing is not tested by cycle counting. This assumption can be bolstered if (1) the cycle counts are approximately consistent with magnetobiochronology or other age information, (2) the cycles can be shown to be periodic, and (3) the lithologic proxy being used is shown to vary in response to orbital forcing in a similar sedimentary environment.

Cycles are expressed as lithologic changes in sedimentary sections. In order to determine whether such cyclicity is periodic it is necessary to parameterize the lithology. One option is to assign a numerical scale to sediment type and simply characterize the lithology with a number (e.g. [4]). Because it is labor-intensive to generate a high-resolution log in this manner, it is more common to use a core or downhole geophysical log as a lithologic proxy. By default, magnetic susceptibility, GRAPE and spectrophotometer logs have been used because they are rapidly generated with a minimum of equipment (e.g. [3]).

The oxygen isotope records that have been used to calibrate the Plio–Pleistocene APTS are a more direct proxy for Earth's climate (as reflected by the size of continental ice sheets) rather than for lithology. The spectral pattern of variations in $\delta^{18}O$ and consistency with climate models have conclusively demonstrated that these records reflect orbital forcing of climate [1,3,5,10]. They can therefore be taken as a 'standard' example of orbital forcing in a sediment sequence. During the Plio–Pleistocene prior to 1 Ma, obliquity (41 kyr) forced fluctuations in the size of ice sheets resulted in variations in $\delta^{18}O$ of amplitude 0.7–1.0‰ [5] while during the late Oligocene this amplitude was only 0.5–0.6‰ [13]. It is likely that $\delta^{18}O$ measurements are not sufficiently sensitive to resolve orbitally forced changes in early Paleogene ice sheets; even if ice sheets existed during the Paleocene–Eocene they were small and would result in <0.3‰ variations in $\delta^{18}O$ on a Myr timescale [14]. Moreover, using $\delta^{18}O$ in this manner requires closely spaced ($\sim$2–4 kyr) samples and is time consuming and expensive. Hence, the development of cyclostratigraphy virtually requires a cheap, rapid geophysical log.

The effort to use cyclostratigraphy as a correlation tool is hindered by the lack of high-resolution geophysical logs for many of the Deep Sea Drilling Project (DSDP) and Ocean Drilling Program (ODP) sections that have become widely used for paleoceanographic reconstruction, especially in the older record. This study addresses that problem by exploiting the archive of high-quality color core photographs that are available for all DSDP and ODP cores. It is shown here that, by digitizing these photographs, it is possible to generate a high-resolution, accurate sediment color log with minimal effort. Previous studies have used core photographs to generate gray-scale reflectance logs useful for cyclostratigraphic (e.g. [12,15]) and sedimentologic (e.g. [16]) analysis. This study builds on that work by (1) demonstrat-

ing that background lighting effects can be corrected, allowing more rigorous analysis of the spectral content of the logs, and (2) utilizing the color information contained in core photographs rather than simply gray-scale.

The spectrophotometer log available for ODP Hole 1051A [17] provides a direct means of evaluating the accuracy of logs generated from core photographs as a measurement of sediment color. Because the spectrophotometer log and the log generated from core photographs measure the same parameter (sediment color) on the same core, correlation between them should be high regardless of the forcing mechanism or sedimentation rate changes. The method also produces similar results to recently published XRF Fe and Ca intensity logs [3] in a ~7 m section in ODP Hole 690B.

1.1. Latest Paleocene–earliest Eocene chronostratigraphy

I demonstrate the potential utility of color logs by constructing a cycle-based correlation between the latest Paleocene–earliest Eocene (magnetic polarity Chron C24r) sections in ODP Holes 690B and 1051A (Fig. 1). Chron C24r has received special attention recently for two primary reasons: (1) It contains the latest Paleocene thermal maximum (LPTM), a runaway greenhouse event that has been the subject of intensive study over the last decade (e.g. [18–21]). (2) It contains the Paleocene/Eocene Series boundary and all candidate levels being considered by the International Global Correlation Project (IGCP) Project 308 for redefinition of the P/E boundary (e.g. [22]). The sections from ODP Sites 690 and 1051 are crucial both to the study of the LPTM (e.g. [18,21,23–25]) and to the construction of a Chron C24r chronostratigraphy (e.g. [24,26]). However, logs suitable for cyclostratigraphic analysis have only been available for Site 1051.

Attempts at magnetobiostratigraphic correlation between Chron C24r sections have concluded that very few, if any, sections are complete through all of Chron C24r [26,27]. As a result, stratigraphic correlation between sites has not been straightforward. The BKSA95 calibration of biostratigraphic data within Chron C24r and the calibration for the age of the LPTM by Aubry et al. [26] (Fig. 1) relies on splicing the sections from Hole 690B and DSDP Hole 550 using biostratigraphic and isotopic correlation [26,28]. The interpolation of ages within the 690B-550 composite section must be tested by constructing a cycle-based chronostratigraphy.

In constructing the 690B-550 composite section, it was realized that the 55 Ma tiepoint used in estimating the seafloor spreading history that forms the basis for the GPTS was substantially in error. This age was calculated for the NP9/NP10 contact at DSDP Site 550 by extrapolating sedimentation rates down from two $^{40}Ar/^{39}Ar$-dated ash layers which occur within Zone NP10 [29]. Aubry et al. [26] determined that the NP9/NP10 contact is unconformable at Hole 550 and that the tiepoint used in constructing the GPTS was misplaced. In order to maintain consistency with both the GPTS and the original radiometric dates at Hole 550, the NP9/NP10 Zonal boundary was fixed at 55 Ma in BKSA95, despite the recognition that this was inconsistent with extrapolation of sedimentation rates derived from magnetostratigraphy [26,28]. As a result, the durations

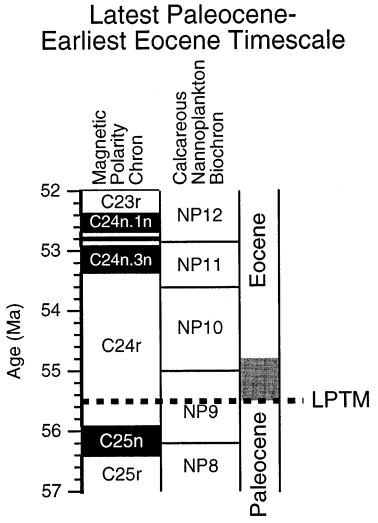

Fig. 1. Integrated magnetobiostratigraphic timescale for the latest Paleocene–earliest Eocene (after [7], with the age of the LPTM from [26]).

of Zones NP9 and NP10 given in BKSA95 were almost guaranteed to be wrong.

Recently, a section was drilled at Site 1051 that is likely complete through Chron C24r and appears to have a good magnetic polarity record [17]. A cyclostratigraphic calibration of the age of the LPTM relative to the base of Chron C24r has been proposed using magnetic susceptibility and Fe intensity logs at Site 1051 [24]. This was the first application of cyclostratigraphy in Chron C24r, primarily because nearly all other LPTM sites lack high-resolution geophysical logs. Fe and Ca intensity logs have also been generated for a ~7 m section containing the LPTM in Hole 690B and were used to facilitate cycle-based correlation of the LPTM interval between Sites 690 and 1051 [25]. The cycle-based age of ~54.94–54.96 Ma for the LPTM is at odds with the estimate of 55.52 Ma based on interpolation of sedimentation rates between the base of C24r and the top of Zone NP9 at Site 690 [26]. It is also at odds with the 55 Ma age assigned to the base of Zone NP10 [7,26], a level which is stratigraphically above (and therefore must be younger than) the LPTM.

2. Methods

Core photographs (35 mm color slides) obtained from ODP were digitized using a flatbed scanner at a resolution of 1200 ppi (pixels per inch), which results in a scaling of approximately 1 pixel in the digitized photograph per mm in the actual core. Each photograph displays one ODP core, with sections of the core arranged parallel to one another (Fig. 2). Individual sections were cropped from the photograph using Adobe Photoshop 4.0 for Macintosh and rescaled with a standard scaling factor of 1 pixel per mm in the actual core (a 1.5 m section is then 1500 pixels long). Processing of the photographs into a color log was performed using a macro written for Wavemetrics Igor Pro 3.14 for Macintosh. Color logs reflect the mean value for each row of pixels in the central 3 cm of each core, resulting in a 'sampling' interval equivalent to 1 mm. The resulting log contains three channels, representing

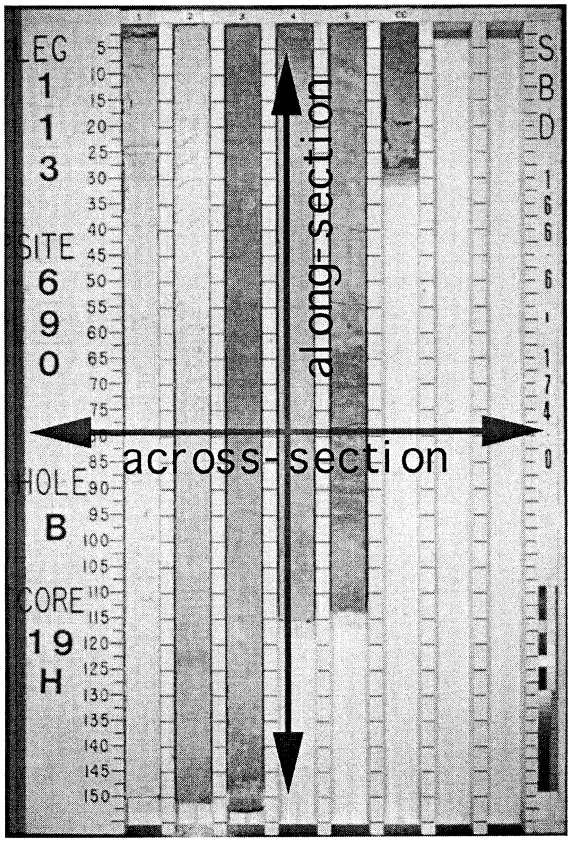

Fig. 2. Illustration of a typical ODP core photograph. Photographs are obviously darker at the edges than in the center. The model used to correct for this lighting effect is illustrated by the arrows: correction is first made for along-section variations in lighting and then for variations in lighting between sections.

red, green, and blue (RGB) values of the digitized photograph.

The effects of lighting are clearly visible in the photographs, with the edges of the photograph darker than the center, and the bulk of the processing macro is devoted to correcting for the background lighting. I remove the background using a simplistic model in which it is assumed that the lighting effects can be characterized by two third-degree polynomials, one along-section and one across-section (Fig. 2). Third-degree polynomials are appropriate because the lighting effect results from a line rather than a point source. The along-section background is approximated by averaging all sections from a single core and per-

forming a least-squares fit of a third-degree polynomial to the resulting curve. The across-section background is approximated by calculating a mean value for each section (after correcting for along-section background), identifying these values by tray position in the photograph, and performing a least-squares fit to the resulting distribution of values for all cores analyzed from an individual hole. Although this model is not sophisticated, it is sufficient for the cores analyzed here.

Core depths (mbsf: meters below seafloor) were adjusted by removing all voids and contracting cores for which the measured length is longer than the drilled length (adjusted depths are given the units 'ambsf'). This preserves the logged depth at the top of every core. For analysis, I have resampled the logs at 2 cm (using adjusted depths) equivalent sampling interval by taking the mean value in each 2 cm length.

Separate Blackman–Tukey spectra using a triangular window were calculated for each of the RGB channels and then averaged to obtain a spectral estimate for the lithologic variations. Evolutive spectra were calculated using a window length of 10 m with a step of 5 m between analyses. A Gaussian filter was used to remove variation with wavelength >10 m prior to calculation of evolutive spectra.

Because cycle counting provides no significance test for cycle recognition, there is an inherent error due to non-cyclic variations (i.e. 'noise') in lithology. In order to estimate the magnitude of this error, minimum and maximum cycle counts were made using conservative and liberal criteria for cycle recognition. Bandpass filters were designed to visually enhance the dominant cyclicity in each section; a large bandwidth was used to minimize 'forcing' the signal into the wavelength of the filter. Counting was performed on the original logs, using filtered logs as a reference. An estimate was made for the number of cycles missing in coring gaps based on an assumption of constant cycle length. Cycle counts were converted to temporal duration by assuming an average precessional cycle length of 0.021 Myr [12].

Published magneto- and biostratigraphies were used to tie the cyclostratigraphy to the integrated magnetobiostratigraphic timescale [7] (Table 1). Calcareous nanoplankton biozonations were assigned using the definitions of Martini [30] as discussed in BKSA95 and Aubry et al. [26]. For Hole 690B, calcareous nanoplankton biostratigraphy was taken from Aubry et al. [26] and Pospichal and Wise [31]. Ali et al. [32] made a careful paleomagnetic study of Hole 690B and concluded that the polarity record primarily represents a drilling overprint rather than the original magnetization of the sediment. The extent of Chron C24r in the section is obscured by this overprint. For Hole 1051A, the calcareous nanoplankton biostratigraphy and magnetostratigraphy were taken from the Site Report [17]. The LPTM can also be used as a point of stratigraphic correlation. The level of the LPTM in Hole 690B was taken from [18]. Although the LPTM occurs in a coring gap in Hole 1051A, the event was recovered at Hole 1051B [21,23]. The error introduced by extrapolation to the level of the LPTM within the coring gap in Hole 1051A is minimal and can be evaluated by comparison with the analysis of Norris and Röhl [24]. Hole 1051A was used here rather than Hole 1051B because of the better delineation of magnetic polarity reversals and biostratigraphic zones in the former. For the sake of simplicity I assume that all magnetobiostratigraphic horizons are associated with discrete depths (Table 1), ignoring error in the location of those horizons.

Table 1
Levels used for stratigraphic correlation in Holes 1051A and 690B

Stratigraphic datum levels				
Datum	Hole 1051A depths		Hole 690B depths	
	mbsf	adj. mbsf	mbsf	adj. mbsf
Base C24n	450.75	450.677	–	–
Base NP11	460.65	460.611	137.8	137.652
Base NP10	–	–	148.9	148.874
LPTM	coring gap	513	170.26	170.26
Base C24r	524.5	524.5	–	–
Base NP9	528.95	528.815	185.9	185.9

Note that errors due to sampling interval are ignored here and in the discussion in the text. The level of the LPTM is approximated based on the record in Hole 1051B.

3. Evaluation of the accuracy of the logs

3.1. Hole 1051A: comparison with spectrophotometer measurements

Shipboard spectrophotometer measurements for Hole 1051A, taken at 5 cm intervals [17], are available from ODP. The spectrophotometer directly measures the reflected light intensity in 10 nm wavelength bins. The resulting spectrum can be converted into a tricoordinate color space (i.e. RGB) using standard conversion tables [33]. In this case, the standard CIE (Commission Internationale de l'Eclairage) XYZ color space was used.

The RGB logs generated from core photographs are measurements made within a tricoordinate color space. In order to compare this with the spectrophotometer log, one log must be converted into the tricoordinate space of the other. Any tricoordinate color space is a linear transform of any other tricoordinate color space, related by the equation [33]:

$$\begin{bmatrix} R' \\ G' \\ B' \end{bmatrix} = \begin{bmatrix} c_{11} & c_{21} & c_{31} \\ c_{12} & c_{22} & c_{32} \\ c_{13} & c_{23} & c_{33} \end{bmatrix} \begin{bmatrix} R \\ G \\ B \end{bmatrix}$$

Consequently, core photograph RGB values should be related to XYZ values through the equation above. Values for the constants (c_{mn}) in this equation must be determined empirically, because they depend on uncontrolled factors such as lighting conditions at the time the photographs were taken, the film used, and the development process. The constants were determined by least-squares fit of the XYZ values to the RGB values, resulting in spectrophotometer logs that can be displayed in color.

There is a very high correlation between sediment color logs from spectrophotometer measurements and core photographs (R (linear correlation

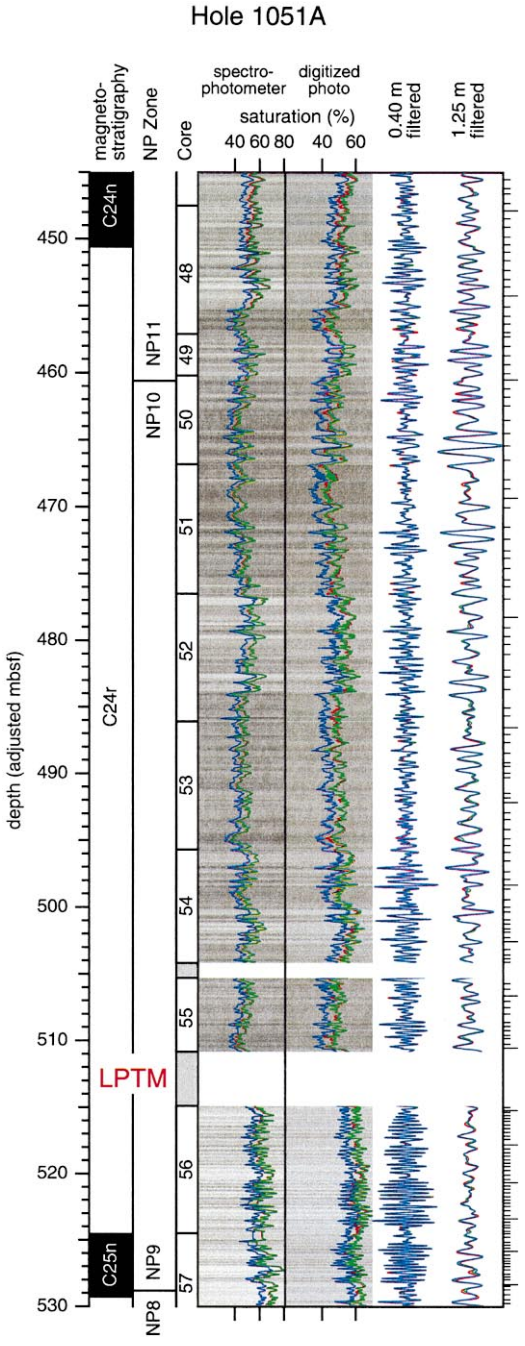

Fig. 3. Hole 1051A spectrophotometer and digitized photograph color logs. The spectrophotometer log has been fitted to the same color space as the digitized photograph log. The rightmost two traces are the digitized photograph color log bandpass filtered with filters centered on 1.25 and 0.40 m wavelength. In the magnetostratigraphy, black represents normal polarity intervals, white represents reversed polarity intervals. Ticks along the right side represent 'best-guess' cycle counts, with every 10th cycle emphasized (emphasis uses an estimated cycle count through coring gaps, to be consistent with Table 2).

coefficient), $R = 0.87$ for red, $R = 0.87$ for blue, $R = 0.89$ for green). Visual examination of the two logs shows that variations in the spectrophotometer logs are of slightly larger amplitude than variations in the logs from digitized photos (dark areas are darker and light areas are lighter; Fig. 3). This may be attributed to a smoothing effect introduced by downsampling the much higher resolution logs from the digitized photos or to the fact that the spectrophotometer gives a linear measure of the intensity of all reflected light while the sensitivity of the slide film is most likely somewhat non-linear with respect to light intensity. In

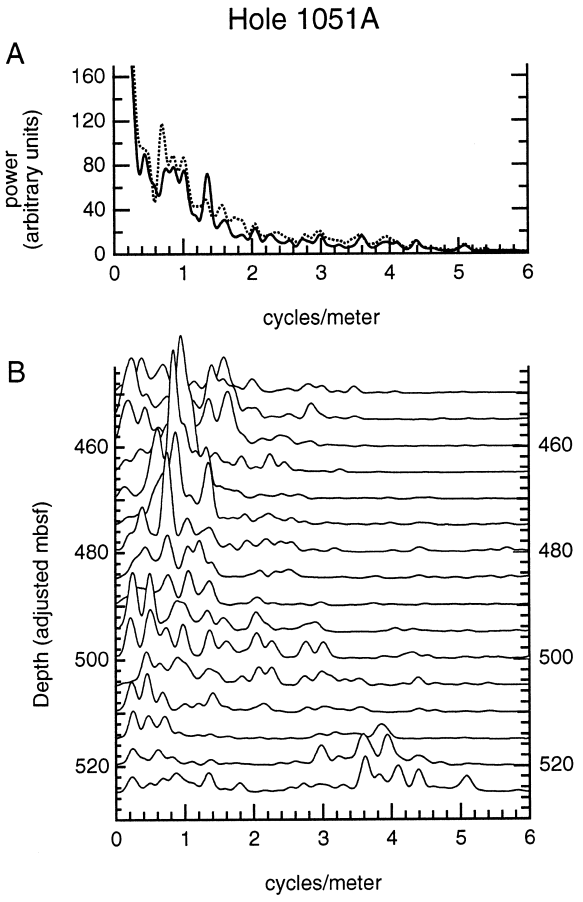

Fig. 4. Power spectra for Hole 1051A. A: Blackman–Tukey power spectrum (lag 10% of series length) for the digitized photograph color log (solid) and the spectrophotometer color log (dashed). B: Evolutive spectrum (lag 70%) for the digitized photograph color log.

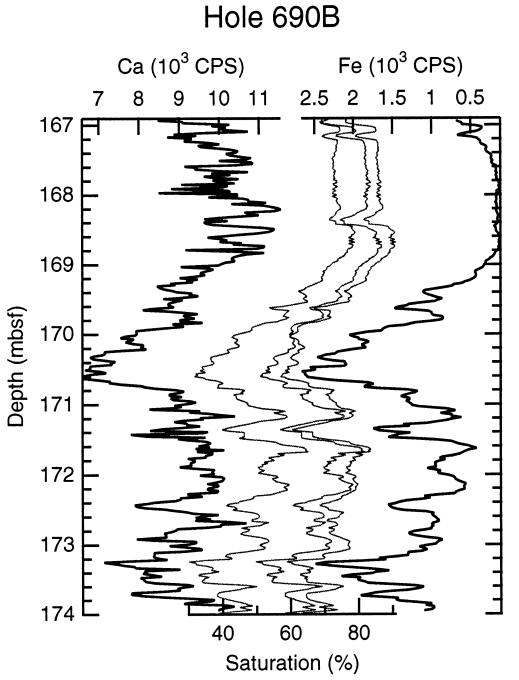

Fig. 5. Lithologic logs for ODP Core 690B-19H. Heavy lines on the left and right are XRF Ca and Fe counts, respectively (from [25]). Thin lines in the center are saturation in RGB color channels (refer to Fig. 6 to identify channels).

any case, this lower amplitude is of no consequence to cyclostratigraphic analysis.

The power spectrum for the spectrophotometer and photograph logs is also essentially identical (Fig. 4A). There is one significant difference between the two spectra: the peak at ~ 0.7 cycles/m (~ 1.4 m wavelength) in the spectrophotometer spectrum is significantly reduced in the digitized photograph spectrum. This is almost certainly the result of the correction for lighting effects at the core section (1.5 m) scale.

3.2. *Hole 690B: comparison with XRF Ca and Fe intensity*

Röhl et al. [25] have published Ca and Fe intensity logs generated using an XRF scanner for the ~ 7 m core containing the LPTM in Hole 690B (core 19H). Sediment color logs generated for the same interval are very similar to these logs, especially to the Fe log (Fig. 5). As Röhl et al. [25] noted, cyclicity disappears in Fe intensity in the

upper part of the section and the color logs are similarly affected. Similar intervals (although typically less severe) contribute to the error in cycle counting.

3.3. Summary

It is clear from the comparison of core photograph and spectrophotometer logs at Hole 1051A that the former is an accurate measure of sediment color. One shortcoming of these logs results from the necessary correction for background lighting: the amplitude of any cyclicity with a wavelength of ~1.5 m will likely be dampened in the color logs. This observation suggests another probable shortcoming: background lighting effects will be more dominant in sections with smaller amplitude variations in sediment color. In the sections analyzed in this study, the amplitude of sediment color variations is large compared with the background lighting effect. It may be more difficult to create usable color logs for sections in which the amplitude of color variations is of the same magnitude as the background lighting effect.

4. Chron C24r cyclostratigraphy

4.1. Results

The most well-developed cyclicity at Hole 1051A occurs at 20–30 cm wavelength between 515 and 525 ambsf and at a wavelength of 75–100 cm between 455 and 485 ambsf (Fig. 3). Cyclicity in the latter interval is not as well developed as in the former. In the evolutive spectrum, the 20–30 cm cyclicity appears as several discrete peaks between 3 and 6 cycles/m; the 75–100 cm cyclicity appears as a high peak between 0.8 and 1 cycles/m with several surrounding peaks (Fig. 4B). The ratio of the peaks between 3 and 6 cycles/m is consistent with that of the several precessional peaks (16, 19 and 23 kyr in the Plio–Pleistocene) caused by modulation of precession by eccentricity. It is difficult to trace these peaks upsection, in part due to the coring gap at 510.5–515 ambsf. One possibility is that the very low amplitude peaks in the range 2–3 cycles/m represent precessional peaks, whereas the high-amplitude peak at ~1 cycle/m is the result of obliquity forcing. Alternatively, there is a large increase in sedimentation rate between 500 and 490 ambsf (as suggested by [24]) and the several peaks in the range 1–2 cycles/m are the result of precessional forcing. It is noted that the ratio of the low frequency peaks is not the same as that of the precessional peaks below 510 ambsf. However, cycle counting indicates that the longer cycles must be precessional: if they were obliquity it would require almost a doubling of the duration of Chron C24r (Table 2). Bandpass filters were designed to isolate cyclicity with wavelength 15–50 cm (6–2 cycles/m) and 60–150 cm (1.7–0.7 cycles/m) (Fig. 3). The filtered

Table 2
Comparison of durations between stratigraphic horizons from referenced timescales [7,9,26] and from cycle counting at Holes 1051A and 690B

Cycle-based interval durations					
Interval	Cycle counts		Durations		
	Hole 1051A	Hole 690B	Timescale	Hole 1051A	Hole 690B
Chron C24r	115–157	–	2.557	2.856 ± 0.441	–
Base NP11-Base C24n	14–17	–	0.26	0.330 ± 0.032	–
Zone NP10	–	25–31	1.39	–	0.588 ± 0.063
LPTM-Base NP10	–	48–60	0.52	–	1.134 ± 0.126
Base C24r-LPTM	41–45	–	0.38	0.903 ± 0.042	–
LPTM-Base NP11	60–95	73–91	1.91	1.628 ± 0.368	1.722 ± 0.189
Base NP9-LPTM	59–64	35–40	0.68	1.292 ± 0.053	0.788 ± 0.053

Ranges reflect only the difference between conservative and liberal cycle counts; errors in the position of magnetobiostratigraphic datums are not incorporated in these estimates.

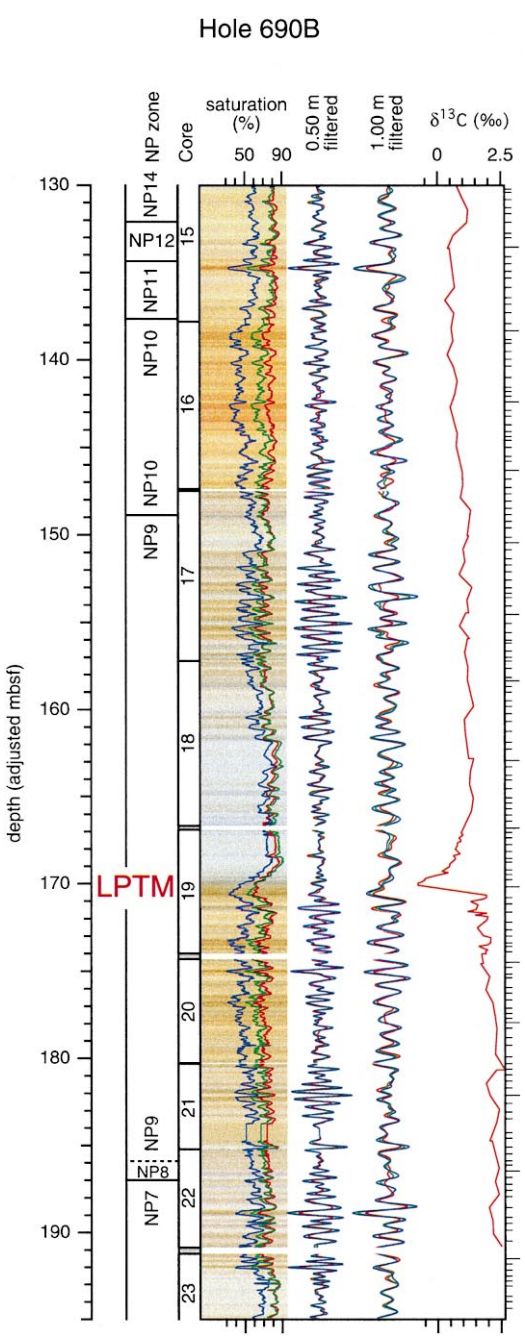

Fig. 6. Hole 690B digitized photograph color logs and benthic foraminiferal $\delta^{13}C$ record (from [18]). The middle two traces are the color log bandpass filtered with filters centered on 1.00 and 0.50 m wavelength. Ticks along the right side represent 'best-guess' cycle counts, with every 10th cycle emphasized.

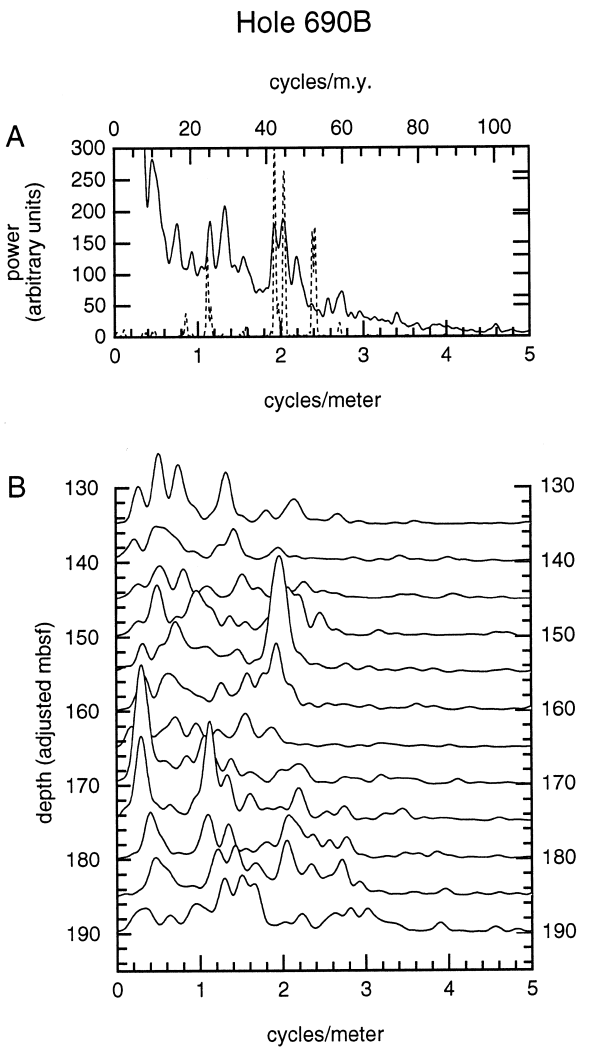

Fig. 7. Power spectra for Hole 690B. A: Blackman–Tukey power spectrum (lag 20%) for the digitized photograph color log (solid, plotted against bottom axis) and calculated mean January insolation at 60°S (dashed, plotted against top axis) [11]. B: Evolutive spectrum (lag 70%) for the color log.

record clearly demonstrates the poorly developed cyclicity in the interval 495–510 ambsf with well-developed short-wavelength cyclicity below and long-wavelength cyclicity above.

At Hole 690B, well-developed cyclicity occurs at wavelengths of 40–60 cm between 150 and 160 ambsf and between 180 and 185 ambsf (Fig. 6). Spectral analysis shows several peaks in this

range (1.7–2.5 cycles/m) that are consistent with precessional forcing (Fig. 7A). Most of the peaks in the spectrum can be explained by Milankovitch forcing with constant sedimentation rate, although there are obvious misfits that suggest some change in sedimentation rate. It is difficult to trace the peaks from the lower part of the section (175–190 ambsf) to the upper part of the section in the evolutive spectrum (Fig. 7B), primarily because of the perturbation caused by the LPTM (~170 ambsf). Therefore, it is difficult to interpret confidently the dominant peak in the spectrum between 150 and 160 ambsf at ~2 cycles/m (50 cm wavelength) as either precessional or obliquity forcing, although if this is an obliquity peak it suggests a large decrease in sedimentation rate between this interval and the section below. Again, because of magnetobiostratigraphic constraints on the duration represented by this interval [7], the cycle count is more compatible with interpreting this as a precessional peak (Table 2). Bandpass filters were designed to isolate 'precessional' cyclicity (30–70 cm wavelength) and 'obliquity' cyclicity (70–130 cm wavelength) (Fig. 6).

Using the identification of cycles and an assumed average cycle duration of 21 kyr, it is possible to reconstruct sedimentation rates throughout the sections analyzed (Fig. 8). While sedimentation rates reconstructed for Hole 690B remain essentially constant at ~2 cm/kyr, sedimentation rates for Hole 1051A more than double from ~1.5 cm/kyr in the lower portion of the section to >3 cm/kyr in the upper portion. These results are consistent with cycle identification made for parts of these sections by Norris and Röhl [24] and Röhl et al. [25] using Fe and Ca intensity and magnetic susceptibility logs. A minimum and maximum cycle count was made in each section between stratigraphic datums (Table 2). The largest error in the cycle count occurs at Hole 1051A in the interval between 495 and 510 ambsf. The gradual increase in cycle wavelength that occurs in this interval leads to greater uncertainty in cycle identification (Fig. 8). As a result, there is a large discrepancy between 'conservative' and 'liberal' delineation of cycles.

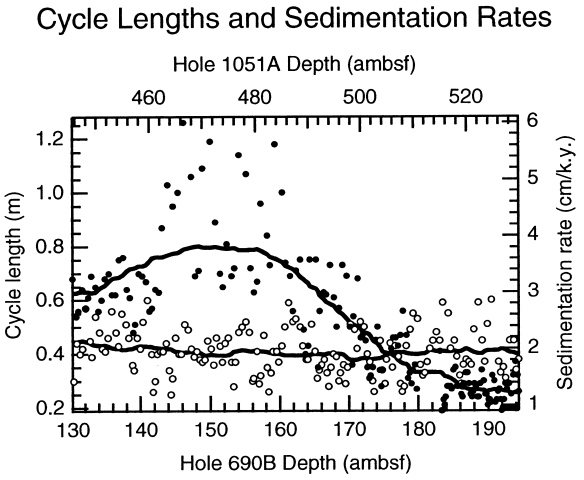

Fig. 8. Cycle length and sedimentation rate through the sections analyzed in Holes 690B (open circles) and 1051A (filled circles). Cycle length was transformed into sedimentation rate using an assumed 21 kyr cycle duration. Individual points represent individual cycles; lines are a 41 point running average. Note that precessional cycles are not expected to be of constant duration, so the running average is more meaningful than the individual points.

4.2. Discussion

Based on the cycle count presented here for Hole 1051A, the LPTM is 903 ± 42 kyr younger than the base of Chron C24r (Table 2). This is consistent with the estimate of 924–966 kyr made by Norris and Röhl [24] using magnetic susceptibility and Fe intensity logs for Site 1051. It contrasts with the estimate of ~480 kyr made by Aubry et al. [26] based on interpolation of sedimentation rates in Hole 690B. The estimate made here is less accurate than that of Norris and Röhl [24] because the LPTM occurs in a coring gap in Hole 1051A; Norris and Röhl [24] spliced logs from Holes 1051A and 1051B to cover this gap. The full duration of Chron C24r at Hole 1051A (2.856 ± 0.441 Myr) is not very well constrained due to uncertainty in cycle identification caused by the gradual increase in cycle length in the interval above the LPTM (Fig. 8). Although the mean duration calculated for Chron C24r is longer than the duration estimated in the GPTS, the cycle-based estimate for the duration of Chron C24r cannot be used to evaluate the accuracy of

the GPTS because of this large error on the cycle counts (Table 2).

The carbon isotope excursion (CIE) which marks the onset of the LPTM can be assumed to be globally synchronous and this event together with the cyclostratigraphy can therefore be used to correlate Holes 1051A and 690B (Fig. 9). There are two reasons to make this correlation. (1) The NP9/NP10 boundary is not delineated in published data from Hole 1051A. The cycle count at Hole 690B allows a calibration for this biostratigraphic datum. (2) The error in cycle counting is much smaller in Hole 690B in the interval above the LPTM. Correlation between the two sites and creation of a 'spliced' section allows a more accurate estimate for the duration of Chron C24r. The magnetostratigraphy for Hole 690B is strongly overprinted and so the cyclostratigraphy can not be directly tied to magnetostratigraphy [32]. The quality of magnetobiostratigraphic data available for Holes 690B and 1051A is typical of Chron C24r sections. No single section can be relied on to produce a standard (chrono)stratigraphy. Instead, it will be necessary to tie numerous sections together using available magnetobiostratigraphic data and test the resulting correlations through cycle-based estimates of temporal duration. The analysis presented here is intended to represent a preliminary step in this process which will be further advanced as more data become available.

In order to splice the sections a second correlation level must be used in conjunction with the CIE. Because the biostratigraphy at Hole 1051A is incomplete, the only level that can be used is the NP10/NP11 contact. This introduces a substantial amount of uncertainty because it has been inferred that biochron NP10 is not completely represented in Hole 690B [26,27]. However, because the cycle-based duration between the LPTM and the base of Zone NP11 is consistent at both sites (Table 2) it is likely that the duration of any hiatuses in Hole 690B must be less than the error in the cycle counts. Eventually, the duration of these inferred hiatuses and the timescale on which diachrony of biostratigraphic data is important can be tested using cycle-based correlation with other sections. For simplicity, the

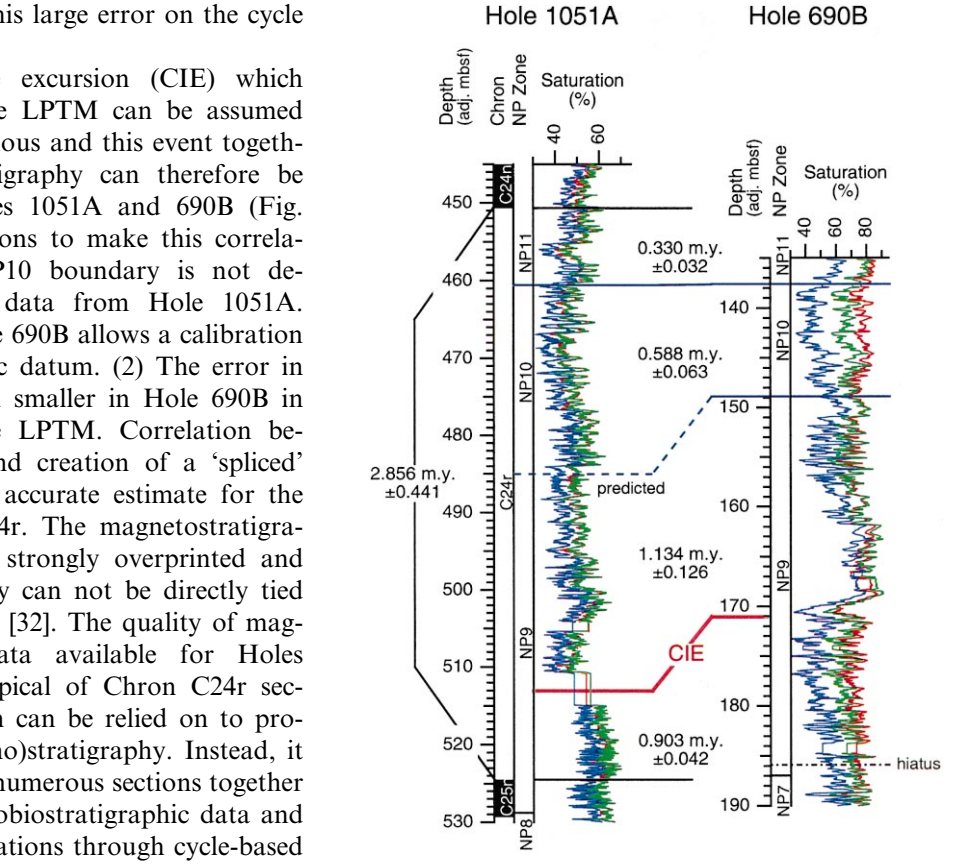

Fig. 9. Correlation between Holes 1051A and 690B. The correlation allows a more precise calculation for the duration of Chron C24r and calculation for the duration between the NP9/NP10 boundary (which is not delineated at Site 1051) and other stratigraphic datums. Note that the position of the Zone NP9/NP10 boundary in Hole 1051A is predicted based on cycle correlation with Hole 690B.

interval between the LPTM and the base of Zone NP11 is taken to be complete in Hole 690B in this discussion.

The duration of Chron C24r should be equivalent to (or slightly longer than) the summed durations in the spliced section of the intervals Base NP11-Base C24n (1051A), NP10 (690B), LPTM-Base NP10 (690B), and Base C24r-LPTM (1051A) (Table 2, Fig. 9). The total duration of this spliced section is 2.955 ± 0.263 Myr, within the error for the Chron C24r cycle count at Hole 1051A. However, this duration is 5–25% longer than the duration estimated in the GPTS.

This duration may be an underestimate because the duration of any hiatuses within Zone NP10 in Hole 690B are not included.

Both the cycle count in Hole 1051A and the duration in the spliced 690B-1051A section suggest that Chron C24r may be 300–400 kyr longer than the 2.557 Myr duration estimated in the GPTS. However, it is likely that this discrepancy is at least partially due to other factors, including: (1) The limits of Chron C24r may be incorrectly delineated at Hole 1051A. (2) Biostratigraphic datums may be diachronous between Holes 1051A and 690B, so that the record is incorrectly spliced. (3) The duration of an average precessional cycle may have been shorter than 21 kyr at 55 Ma. It would be premature to conclude that any one of these factors is primarily responsible for the discrepancy based on the data presented here. The duration for Chron C24r estimated in the GPTS is much more robust than any estimate that could be made based on existing cyclostratigraphic data.

The following testable hypotheses can be drawn from the correlation between Holes 1051A and 690B (Fig. 9):

1. A ~500 kyr hiatus occurs in the interval between the base of NP9 and the LPTM in Hole 690B, accounting for the difference in the number of cycles between these two data in Holes 690B and 1051A (Table 2, Fig. 9). Zone NP8 is very thin in Hole 690B, suggesting that the hiatus is longer than 500 kyr and encompasses most of Zone NP8 and the base of Zone NP9. As a result, the age estimate for the LPTM based on the assumption of a conformable NP8/NP9 boundary and good magnetostratigraphy at Site 690B [26] is too old.
2. The duration of nannofossil Zone NP9 was greatly underestimated and the duration of NP10 was overestimated in BKSA95 (Table 2, Fig. 9). Zone NP9 is ~2.4 Myr long (rather than 1.18 Myr) and NP10 is ~0.6 Myr long (rather than 1.39 Myr). This difference was predictable, since the NP9/NP10 Zonal boundary was forced to be 55 Ma in order to be consistent with certain assumptions made in constructing the GPTS (see above). The error introduced into the GPTS by using the 55 Ma tiepoint can be estimated (very roughly) by examining the cyclostratigraphic calibration presented here. The $^{40}Ar/^{39}Ar$ date for the lower ash layer at Hole 550 is 54.51 ± 0.05 Ma. Because this ash layer occurs within Zone NP10 it provides a constraint on the minimum age at the base of that zone. Using 54.6 Ma for the base of Zone NP10 and the cycle-based durations, the top of Chron C24r is ~53.7 Ma rather than 53.347 Ma as given in the GPTS. The age of the LPTM would then be between 55.3 and 55.7 Ma, depending on the total duration used for Chron C24r.
3. The NP9/NP10 boundary should be found at ~485 mbsf in Hole 1051A (Fig. 9). This prediction is made based on cycle counting down from the NP10/NP11 boundary but is consistent with counting up from the LPTM.

4.3. Future work

Using only Holes 1051A and 690B it is impossible to improve the age calibrations for the GPTS in this interval because there is no independent age for any level in either section. In order to modify the GPTS it will be necessary to directly tie a cyclostratigraphy to the $^{40}Ar/^{39}Ar$ dates using Hole 550 or another section with datable ash layers. Similarly, diachrony of biostratigraphic datums cannot be evaluated using the data presented here because the errors in the cycle count are too large and published biostratigraphies for Hole 1051A do not permit full delineation of all zones and subzones recognized by Aubry et al. [26,27] in Hole 690B.

Although cycle counts can be very accurate, there is no means of estimating that accuracy other than making a conservative and liberal count as I have done. A more robust, astronomically based chronostratigraphy can be produced by tuning logs to exploit the full spectrum predicted by orbital theory [3,4,11]. Ultimately, the test of any timescale is consistency between geographically separate sections. This can only be gauged through attempted correlation between available sections, even when the points of correlation are not ideal. Using sediment color logs from core

photographs will greatly advance this process by providing a means to 'retrofit' high-resolution lithologic logs for many sections which have become crucial for paleoceanography and chronostratigraphy.

5. Conclusions

Color logs produced by digitizing core photographs provide an easy means of generating high-resolution geophysical logs for ODP and DSDP sites which lack such logs. This method will be useful for cyclostratigraphic calibration of many sites which were drilled before core and downhole logging was standard practice. The logs are reliable both as absolute measures of sediment color and as accurate recorders of sediment cyclicity, although the amplitude of cyclicity at the core section (1.5 m) scale is somewhat dampened.

The discrepancy between the cycle counts in the Chron C24r sections at Holes 1051A and 690B and the GPTS is fairly small, but too large to be reconciled based solely on the data from these two sections. The astronomically calibrated durations of calcareous nannofossil zones within Chron C24r presented here is substantially different from that in BKSA95 and Aubry et al. [26]. Using color logs generated from core photographs will make it significantly easier to test these calibrations in other sections and, eventually, to revise the GPTS in this interval. Because chronostratigraphy provides the sole means of assessing rates and relative timing of climate processes, it can be expected that future, astronomically based revisions to the timescale will have repercussions in the interpretation of Earth's climate history in the late Paleocene–early Eocene.

Acknowledgements

I thank Ken Miller, Dennis Kent, and Marie Aubry for instigating this study, for many helpful suggestions and discussions and, with Mimi Katz and Luca Lanci, for comments on the manuscript. Tim Herbert and Ellen Thomas provided very useful and thorough reviews of the manuscript. This material is based upon work supported under a National Science Foundation Graduate Research Fellowship. *[RV]*

References

[1] J.D. Hays, J. Imbrie, N.J. Shackleton, Variations in the Earth's orbit pacemaker of the ice ages, Science 194 (1976) 1121–1132.

[2] F.J. Hilgen, W. Krijgsman, C.G. Langereis, L.J. Lourens, A. Santarelli, W.J. Zachariasse, Extending the astronomical (polarity) time scale into the Miocene, Earth Planet. Sci. Lett. 136 (1995) 495–510.

[3] N.J. Shackleton, S. Crowhurst, T. Hagelberg, N.G. Pisias, D.A. Schneider, A new Late Neogene time scale: application to Leg 138 Sites, in: N.G. Pisias, L.A. Mayer, T.R. Janecek, A. Palmer-Julson, T.H. van Andel (Eds.), Proc. ODP, Sci. Results 138, Ocean Drilling Program, College Station, TX, 1995, pp. 73–101.

[4] P.E. Olsen, D.V. Kent, Milankovitch climate forcing in the tropics of Pangaea during the Late Triassic, Paleogeogr. Paleoclimatol. Paleoecol. 122 (1996) 1–26.

[5] N.J. Shackleton, A. Berger, W.R. Peltier, An alternative astronomical calibration of the lower Pleistocene based on ODP Site 677, Trans. R. Soc. Edinb. 81 (1990) 251–261.

[6] P.R. Renne, A.L. Deino, R.C. Walter, B.D. Turrin, C.C. Swisher, T.A.G. Becker, H. Curtis, W.D. Sharp, A.R. Jaouni, Intercalibration of astronomical and radioisotopic time, Geology 22 (1994) 783–786.

[7] W.A. Berggren, D.V. Kent, C.C. Swisher, III, M.-P. Aubry, A revised Cenozoic geochronology and chronostratigraphy, in: W.A. Berggren, D.V. Kent, M.-P. Aubry, J. Hardenbol (Eds.), Geochronology Time Scales and Global Stratigraphic Correlation, Spec. Publ., 54, SEPM, Tulsa, OK, 1995, pp. 129–212.

[8] S.C. Cande, D.V. Kent, A new geomagnetic polarity time scale for the Late Cretaceous and Cenozoic, J. Geophys. Res. 97 (1992) 13917–13951.

[9] S.C. Cande, D.V. Kent, Revised calibration of the geomagnetic polarity time scale for the Late Cretaceous and Cenozoic, J. Geophys. Res. 100 (1995) 6093–6095.

[10] J. Imbrie, J.D. Hays, D.G. Martinson, A. McIntyre, A.C. Mix, J.J. Morley, N.G. Pisias, W.L. Prell, N.J. Shackleton, The orbital theory of Pleistocene climate: support from a revised chronology for the marine $\delta^{18}O$ record, in: A. Berger, J. Imbrie, J. Hays, G. Kukla, B. Saltzman (Eds.), Milankovitch and Climate (Suppl. 1), D. Reidel, Dordrecht, 1984, pp. 269–305.

[11] J. Laskar, The chaotic motion of the solar system: A numerical estimate of the chaotic zones, Icarus 88 (1990) 266–291.

[12] T.D. Herbert, I. Premoli-Silva, E. Erba, A.G. Fischer, Orbital chronology of Cretaceous–Paleocene marine sediments, in: W.A. Berggren, D.V. Kent, M.-P. Aubry, J. Hardenbol (Eds.), Geochronology Time Scales and Glob-

al Stratigraphic Correlation, Spec. Publ., 54, SEPM, Tulsa, OK, 1995, pp. 81–92.
[13] J.C. Zachos, B.P. Flower, H. Paul, Orbitally paced climate oscillations across the Oligocene/Miocene boundary, Nature 388 (1997) 567–570.
[14] J.V. Browning, K.G. Miller, D.K. Pak, Global implications of lower to middle Eocene sequence boundaries in the New Jersey coastal plain: The icehouse cometh, Geology 24 (1996) 639–642.
[15] T.D. Herbert, S.L. D'Hondt, Precessional climate cyclicity in Late Cretaceous–Early Tertiary marine sediments: A high resolution chronometer of Cretaceous–Tertiary boundary events, Earth Planet. Sci. Lett. 99 (1990) 263–275.
[16] W.S. Broecker, G. Bond, M. Klas, G. Bonani, W. Wolfli, A salt oscillator in the Glacial Atlantic? 1. The concept, Paleoceanography 5 (1990) 469–477.
[17] Shipboard scientific party, Site 1051, in: R.D. Norris, D. Kroon, A. Klaus, et al. (Eds.), Proc. ODP, Inital. Rep., 171B, Ocean Drilling Program, College Station, TX, 1998, pp. 171–239.
[18] J.P. Kennett, L.D. Stott, Abrupt deep-sea warming, palaeoceanographic changes and benthic extinctions at the end of the Paleocene, Nature 353 (1991) 225–229.
[19] J.C. Zachos, K.C. Lohmann, J.C.G. Walker, S.W. Wise, Abrupt climate change and transient climates during the Paleogene: a marine perspective, J. Geol. 101 (1993) 191–213.
[20] G.R. Dickens, M.M. Castillo, J.G.C. Walker, A blast of gas from the latest Paleocene Simulating first-order effects of massive dissociation of oceanic methane hydrate, Geology 25 (1997) 259–262.
[21] M.E. Katz, D.K. Pak, G.R. Dickens, K.G. Miller, The source and fate of massive carbon input during the latest Paleocene thermal maximum, Science 286 (1999) 1531–1533.
[22] M.-P Aubry, Where should the global stratotype section and point (GSSP) for the Paleocene/Eocene be located?, Bull. Geol. Soc. Fr. 171 (2000) 461–476.
[23] S. Bains, R.M. Corfield, R.D. Norris, Mechanisms of climate warming at the end of the Paleocene, Science 285 (1999) 724–727.
[24] R.D. Norris, U. Röhl, Carbon cycling and chronology of climate warming during the Palaeocene/Eocene transition, Nature 401 (1999) 775–778.
[25] U. Röhl, T.J. Bralower, R.D. Norris, G. Wefer, New chronology for the late Paleocene thermal maximum and its environmental implications, Geology 28 (2000) 927–930.
[26] M.-P. Aubry, W.A. Berggren, L. Stott, A. Sinha, The upper Paleocene–lower Eocene stratigraphic record and the Paleocene–Eocene boundary carbon isotope excursion: Implications for geochronology, in: R.W. O'B. Knox, R.M. Corfield, R.E. Dunay (Eds.), Correlation of the Early Paleogene in Northwest Europe, Spec. Publ., 101, Geol. Soc. Lond., 1996, pp. 353–380.
[27] M.-P. Aubry, B.S. Cramer, K.G. Miller, J.D. Wright, D.V. Kent, R.K. Olsson, Late Paleocene event chronology: unconformities, not diachrony, Bull. Soc. Géol. Fr. 171 (2000) 367–378.
[28] M.-P. Aubry, Stratigraphic (dis)continuity and temporal resolution of geological events in the upper Paleocene–lower Eocene deep sea record, in: M.-P. Aubry, S. Lucas, W.A. Berggren (Eds.), Late Paleocene–Early Eocene Climatic and Biotic Events in the Marine and Terrestrial Records, Columbia University Press, New York, 1998, pp. 37–66.
[29] C.C. Swisher, III, R.W.O'B. Knox, The age of the Paleocene/Eocene boundary: $^{40}Ar/^{39}Ar$ dating of the lower part of NP10, North Sea Basin and Denmark (abstract), in: IGCP 308 (Paleocene/Eocene boundary events), International Annual Meeting and Field Conference, 2–6 December 1991, Brussels, Abstracts with Program, 1991, p. 16.
[30] E. Martini, Standard Tertiary and Quaternary calcareous nannoplankton zonation, in: Farinacci, A (Ed.), Proceedings of the Second Planktonic Conference, 1971, pp. 739–761.
[31] J.J. Pospichal, S.W. Wise, Paleocene to middle Eocene calcareous nannofossils of ODP Sites 689 and 690, Maud Rise, Weddell Sea, in: P.F. Barker, J.P. Kennett et al. (Eds.), Proc. ODP, Sci. Results, 113, Ocean Drilling Program, College Station, TX, 1990, pp. 613–666.
[32] J.R. Ali, D.V. Kent, E.A. Hailwood, Magnetostratigraphic reinvestigation of the Paleocene/Eocene boundary interval in Hole 690B, Maud Rise, Antarctica, Geophys. J. Int. 141 (2000) 639–646.
[33] G. Wyszecki, W.S. Stiles, Color Science: Concepts and Methods, Quantitative Data and Formulae, 2nd edn., John Wiley and Sons, New York, 1982, 950 pp.